Load and Time Dependence of Interfacial Chemical Bond-Induced Friction at the Nanoscale

Kaiwen Tian,[1] Nitya N. Gosvami,[2,†] David L. Goldsby,[3] Yun Liu,[4] Izabela Szlufarska,[5] and Robert W. Carpick[2,*]
[1]Department of Physics and Astronomy, University of Pennsylvania, Philadelphia, Pennsylvania 19104, USA
[2]Department of Mechanical Engineering and Applied Mechanics, University of Pennsylvania, Philadelphia, Pennsylvania 19104, USA
[3]Department of Earth and Environmental Sciences, University of Pennsylvania, Philadelphia, Pennsylvania 19104, USA
[4]Department of Chemistry and Chemical Biology, Harvard University, Cambridge, Massachusetts 02138, USA
[5]Department of Materials Science and Engineering, University of Wisconsin–Madison, Madison, Wisconsin 53706, USA
(Received 19 March 2016; revised manuscript received 8 July 2016; published 16 February 2017)

Rate and state friction (RSF) laws are widely used empirical relationships that describe the macroscale frictional behavior of a broad range of materials, including rocks found in the seismogenic zone of Earth's crust. A fundamental aspect of the RSF laws is frictional "aging," where friction increases with the time of stationary contact due to asperity creep and/or interfacial strengthening. Recent atomic force microscope (AFM) experiments and simulations found that nanoscale silica contacts exhibit aging due to the progressive formation of interfacial chemical bonds. The role of normal load (and, thus, normal stress) on this interfacial chemical bond-induced (ICBI) friction is predicted to be significant but has not been examined experimentally. Here, we show using AFM that, for nanoscale ICBI friction of silica-silica interfaces, aging (the difference between the maximum static friction and the kinetic friction) increases approximately linearly with the product of the normal load and the log of the hold time. This behavior is attributed to the approximately linear dependence of the contact area on the load in the positive load regime before significant wear occurs, as inferred from sliding friction measurements. This implies that the average pressure, and thus the average bond formation rate, is load independent within the accessible load range. We also consider a more accurate nonlinear model for the contact area, from which we extract the activation volume and the average stress-free energy barrier to the aging process. Our work provides an approach for studying the load and time dependence of contact aging at the nanoscale and further establishes RSF laws for nanoscale asperity contacts.

DOI: 10.1103/PhysRevLett.118.076103

Friction is important in a wide range of technological, industrial, biological, and natural systems [1–3]. One of the most general approaches describing macroscale friction is the rate and state friction (RSF) formalism [4–10]. Often deemed "laws," RSF laws are actually empirical and lack a robust physical basis. In spite of this, RSF laws fit friction data for a remarkably wide range of materials including paper [11], organic monolayer-coated microelectromechanical systems [1–3], and granular media and rocks [4,6,8,11–14].

The RSF laws include an evolution effect where the contact behavior evolves with time. This leads to the static friction force increasing logarithmically with the hold time. This manifestation of the evolution effect, known as aging, has been observed for many macroscale experiments for hold times from 0.1 to 10^5 s [4,5,8,9]. Two aging mechanisms have been proposed. The first is an increase in the real contact area (to which friction is proportional [15,16]) with time, due to plastic creep, referred to as the "contact quantity." The second is due to the formation of chemical bonds across the interface, causing an increase in friction, without a change in the contact area, referred to as "contact quality." At the macroscale, many mechanisms may contribute to friction simultaneously, making it difficult to deconvolve their effects. This is one reason why macroscopic RSF laws remain largely empirical.

To isolate the physical mechanisms that underpin RSF laws, Li *et al.* performed single asperity slide-hold-slide (SHS) experiments for single asperity silica-silica nanocontacts using an atomic force microscope (AFM). In these tests, which mimic macroscopic SHS tests on rock samples, the AFM tip, after sliding on the substrate, is then held still for some time, and then it slides again. An amorphous silica tip and substrate were used, because silicate minerals dominate the lithology of crustal rocks and have similar frictional behavior as amorphous silica [17,18]. Static aging was observed without plastic deformation [18], excluding creep. They observed a logarithmic increase of the friction drop ΔF (the difference between the static friction force after holding and the subsequent kinetic friction force) with hold times from 0.1 to 100 s. They proposed that aging was due to interfacial chemical bond formation, which was supported by the fact that no aging occurred when contacts were made under similar or even more severe conditions between silica tips and surfaces resistant to covalent bond formation with silica, namely, diamond and graphite. Liu and Szlufarska's subsequent first-principles calculations showed that covalent interfacial siloxane (Si-O-Si) bridges indeed form at silica-silica interfaces under similar conditions [19].

Of the multiple ways covalent bonds can form between silica surfaces [20], the nanoscale studies proposed an

interfacial siloxane bond (Si-O-Si) formation. This assumes that the silica surfaces are highly hydroxylated and thus hydrophilic. Indeed, the samples were treated with a piranha solution [18] and the experiments conducted in a significant partial pressure of water which will quickly hydroxylate any dangling bonds. In this situation, two silanol (Si-OH) groups from opposing surfaces react to form a siloxane bond:

$$\text{Si-OH} + \text{Si-OH} \rightarrow \text{Si-O-Si} + \text{H}_2\text{O}.$$

Using kinetic Monte Carlo simulations, Liu and Szlufarska also showed that the logarithmic regime of the dependence of the number of bonds on time could span the time scale comparable to the experiments. The existence of a regime of logarithmic dependence was shown to arise from the kinetics of interfacial reactions, and the extent of this regime was found to be significantly affected by elastic strain-induced interactions that inhibit bond formation near existing bonds. Li *et al.* showed using molecular dynamics simulations that the friction force is approximately proportional to the number of siloxane bonds [21], providing a plausible explanation for the observed frictional aging. These results provide the first asperity-level understanding of the interfacial chemical bond-induced (ICBI) friction for silica-silica interfaces.

Since the kinetic friction is not affected by aging, it can be treated as a constant. Therefore, the static friction force studied by Liu and Szlufarska [19] and the friction drop studied by Li *et al.* [18] differ only by a constant offset (the kinetic friction force). Here, we use the friction drop to describe aging.

The simulations of Li *et al.* also studied the effect of load on the static friction of a flat-on-flat silica-silica contact in the tensile regime and found that the maximum static friction is proportional to the normal pressure (equivalent to the normal force, due to the nominally flat geometry) for a given number of interfacial siloxane bonds at a low temperature [21]. To determine if a similar effect occurs in AFM experiments, to further test if the siloxane bridge mechanism occurs, and to further investigate nanoscale RSF behavior, we studied aging vs normal load using piranha-treated (i.e., hydroxylated) silica substrates.

Si AFM tips and Si(001) wafers were thermally oxidized and the wafers hydroxylated using a piranha solution prior to the experiments, which were conducted under a controlled relative humidity at 1 atm in nitrogen gas.

The friction drop ΔF was measured and plotted vs $\log t_{\text{hold}}$ (where t_{hold} is the hold time) for applied normal loads from the lowest load where stable measurements could be conducted to the highest load that could be reached in our instrument. From the same data, ΔF vs the normal load for each of the hold times t_{hold} was plotted (Fig. 1). The approximate linear relation between ΔF and $\log t_{\text{hold}}$ exists for loads from 20 to 400 nN [Fig. 1(a)], with a slope that increases approximately linearly with the load

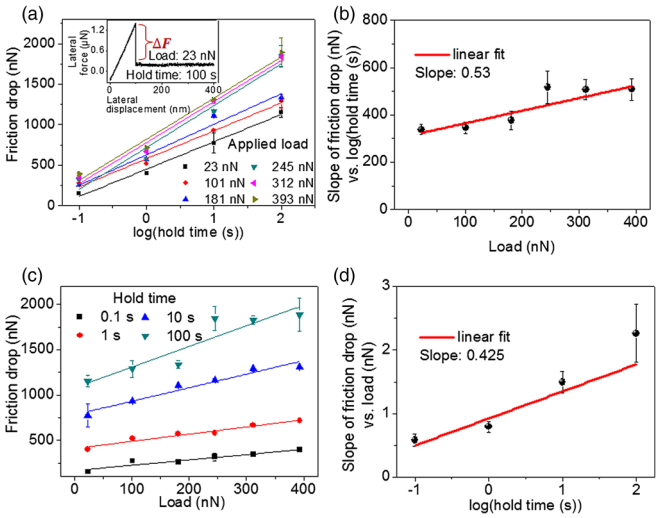

FIG. 1. Effect of the hold time and applied normal load on static aging. Relative humidity (RH) = 53%, temperature $T = 24\,^{\circ}\text{C}$, and the loading point velocity is 500 nm/s. (a) Friction drop vs log of the hold time for different normal loads. The inset shows the lateral force vs lateral displacement curve from the test for 100 s hold time and 23 nN applied load and indicates how we measure the friction drop. The linearity of friction drop vs log of the hold time is seen for all normal loads. (b) The slope of each linear fit in (a) vs the load. The slope varies linearly with the load. (c) Friction drop vs load for different hold times. For a given hold time, the friction drop increases linearly with the load. (d) The slope of the linear fits from (c) vs the log of the hold time. The slope increases linearly with the log of the hold time. Loads and hold times are varied randomly to exclude systematic errors.

[Fig. 1(b)] (small deviations from linearity are seen at the shortest hold time of 0.1 s, in agreement with Liu and Szlufarska [19]; experiments are currently underway at even shorter hold times to investigate this and will be discussed in a separate publication). Correspondingly, for each value of t_{hold}, ΔF increases approximately linearly with the load [Fig. 1(c)], with a slope that increases approximately linearly with $\log t_{\text{hold}}$ [Fig. 1(d)]. For simplicity, henceforth we replace t_{hold} with t. The slopes from Figs. 1(b) and 1(d) are comparable; they are 0.530 and 0.425, respectively. We demonstrate in Supplemental Material Sec. 2 [22] that the linearity in Figs. 1(b) and 1(d) and the slopes of the linear fittings in those two figures being comparable are expected, due to the simultaneous linearity of the friction drop vs load [Fig. 1(a)] and the friction vs $\log t$ [Fig. 1(c)]. The linearity in Figs. 1(a) and 1(c) also implies that the functional dependence of ΔF on $\log(t)$ and on load L should be (see Supplemental Material Sec. 2 [22] for the derivation)

$$\Delta F(L, \log(t)) = h(L + k)(\log(t) + m) + q, \quad (1)$$

where h, k, m, and q are constants.

To develop the physical basis underlying the empirical relationship in Eq. (1), we start by assuming that the reaction

energy barriers for the aging process are uniformly distributed over the range of $[0,G]$, where 0 corresponds to a barrierless reaction and G is the uppermost energy barrier, as done in Refs. [19,21]. The limitations of this assumption are discussed further below. This allows us to derive a simple analytical formula that describes the reaction kinetics of a siloxane bond formation (based on Sec. S5 of Ref. [19], and the details are in Supplemental Material Sec. 8 [22])

$$P(t) = \frac{N}{G} k_B T [2.3 \log(t) - 2.3 \log(\tau_0) + 0.58], \quad (2)$$

where $P(t)$ is the number of reaction sites where siloxane bonds have formed, k_B is Boltzmann's constant, T is the temperature, t is the hold time, N is the number of available reaction sites at the beginning, and τ_0 is the time constant for the siloxane bond formation.

Liu and Szlufarska considered $P(t)$ to be proportional to the static friction force, consistent with previous experiments [37] and supported by simulations [21,38]. We further assume that the maximum force that can be supported by each interfacial bond is equal to the breaking force of a siloxane bond f_0. Thus, $\Delta F = f_0 P(t)$. According to Ref. [39], $f_0 \approx 1.5$ nN.

We also assume that $N = \rho S$, where ρ is the number density of initial available reaction sites and S is the contact area. To apply Eq. (2) to the experimental data (Fig. 1), we need to establish a relationship between contact area S and load L and determine how the uppermost energy barrier G depends on L.

According to the Derjaguin-Müller-Toporov (DMT) model, the contact area $S = \pi[3R(L + L_0)/4E_C]^{2/3}$, where the effective Young's modulus $E_C = [2(1-\nu^2)/E]^{-1}$, E and ν are, respectively, the Young's modulus and Poisson's ratio of silica, and L_0 is the pull-off force (due to adhesion). The average pressure $\sigma = (L + L_0)/S = (1/\pi)(4E_C/3R)^{2/3}(L + L_0)^{1/3}$. Following basic stress-activated kinetics from the transition state theory, we take the uppermost energy barrier when stress is applied to be $G = G_0 - \sigma V_0$ [40–42], where G_0 is the uppermost energy barrier when the contact is stress-free and V_0 is the activation volume. Thus, Eq. (2) becomes

$$\Delta F = f_0 k_B T \rho \pi \left(\frac{3R}{4E_C}\right)^{2/3} \times \frac{(L + L_0)^{2/3}}{G_0 - \frac{V_0}{\pi}\left(\frac{4E_C}{3R}\right)^{2/3}(L + L_0)^{1/3}} \times [2.3 \log(t) - 2.3 \log(\tau_0) + 0.58]. \quad (3)$$

To obtain a simpler expression and extract the desired parameters, we apply two different linear approximations. For the first stage of linearization, we assume that the effect of stress on the uppermost activation barrier G is small, which is consistent with the small activation volume determined later. Assuming G is constant, Eq. (3) becomes

$$\Delta F = \frac{f_0 k_B T \rho \pi}{G} \left(\frac{3R}{4E_C}\right)^{2/3} (L + L_0)^{2/3} \times [2.3 \log(t) - 2.3 \log(\tau_0) + 0.58]. \quad (4)$$

This equation has a convenient form, as it allows us to extract $L_0 = 253$ nN and $\tau_0 = 0.033$ s from the data in Fig. 1 by tuning L_0 and τ_0 so that all the data points in Figs. 1(a) and 1(c) converge as closely as possible onto a single master curve (see Supplemental Material Sec. 3 [22]). The value of $\tau_0 = 0.033$ s$[\log(0.033) = -1.48]$ is larger than the expected atomic vibration period $\sim 10^{-13}$ s $[\log(10^{-13}) = -13]$. We attribute this discrepancy to the assumption of a uniform distribution of the reaction energy barrier in the current analysis. We checked this by performing kinetic Monte Carlo simulations (similar to those reported in Ref. [19]), which assumed a more realistic, nonuniform distribution of energy barriers and considered variable bond strength. These simulations showed that the time span over which the dependence of friction on the log of the hold time is linear is consistent with our experimental results. The details of the extraction of L_0 and τ_0, the simulation, and related discussions are provided in Supplemental Material Sec. 3 [22].

With these values of L_0 and τ_0 in hand, we then use Eq. (3) to fit the data in Fig. 1(c) to obtain G_0 and V_0. We already have $f_0 = 1.5$ nN [39], $k_B T = 4.1 \times 10^{-21}$ J, $R = 130$ nm, $E_C = 35.3$ GPa, $\rho = 4/\text{nm}^2$ [19], $\tau_0 = 0.033$ s, and $L_0 = 253$ nN. For a given value of hold time t, ΔF is thus a function of L, with only two unknown parameters G_0 and V_0. We fit the friction drop vs load data for different hold times in Fig. 1(c) using Eq. (3). For $t = 0.1$ s, we obtain $G_0 = (1.06 \pm 0.21)$ eV and $V_0 = (78 \pm 28)$ Å^3, both of which are physically reasonable values for a chemical bonding mechanism [19,40]. For comparison, Liu and Szlufarska found from the density-functional theory that the typical energy barrier values for siloxane bridging range between 0.5 and 1.4 eV [19]. The fitting curve is shown in Fig. 2. The quality of the fit is not as good

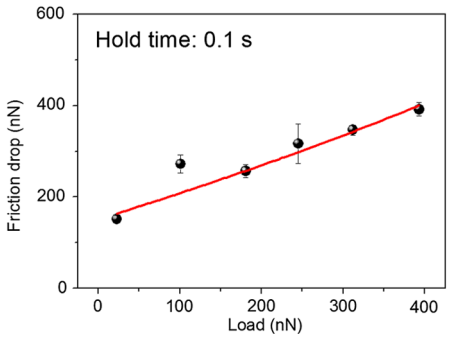

FIG. 2. Fitting of the friction drop vs load. The data points correspond to a hold time of 0.1 s in Fig. 1(c). The fitting is according to Eq. (3). It can be extracted from the fitting that $G_0 = (1.06 \pm 0.21)$ eV and $V_0 = (78 \pm 28)$ Å^3.

for other hold times; all details are presented in Supplemental Material Sec. 11 [22].

For the second stage of linearization, we perform a Taylor expansion of Eq. (4) around $L = 0$. This is equivalent to assuming that the contact area varies linearly with load L. Such an approximation of the kinetic friction (and thus contact area) vs load has been found to be reasonably accurate in several nanoscale friction experiments [43,44]. While seemingly crude, as shown in Supplemental Material Sec. 7 [22], this produces at most an error of 9.1% in the contact area at the highest load used, which is reasonable. This gives

$$\Delta F = \frac{f_0 k_B T \rho \pi}{G}\left(\frac{3R}{4E_C}\right)^{2/3} L_0^{-1/3}\left(\frac{2}{3}L + L_0\right) \times [2.3\log(t) - 2.3\log(\tau_0) + 0.58]. \quad (5)$$

Note that Eq. (5) is a special case of Eq. (1), with $q = 0$. Therefore, we obtain an equation that explains the experimental finding of an approximately linear dependence of the friction drop on load times the log of the hold time.

Note that we do not directly use Eq. (5) to extract L_0 and τ_0 in order to reduce error, since Eq. (4) maintains the nonlinear expression of load according to the DMT model and thus is more accurate than Eq. (5).

To show that this linear approximation is reasonably accurate, we measured the kinetic friction vs load in the positive load regime using another oxidized Si tip on piranha-cleaned silica (Fig. 3), revealing a nearly linear dependence of kinetic friction on the load (with an offset along the load axis due to adhesion). The velocity was large enough to avoid any significant evolution effect. Additional details on the decrease of the magnitude of the evolution effect with a loading point velocity in smooth sliding tests will be presented in a future publication. For a nonaging single-asperity contact, kinetic friction is often observed to be proportional to the contact area S [45], including for silicon and silica contacts [46,47]. This and our results in Fig. 3 demonstrate that the linear approximation of the load dependence of S on L is reasonable.

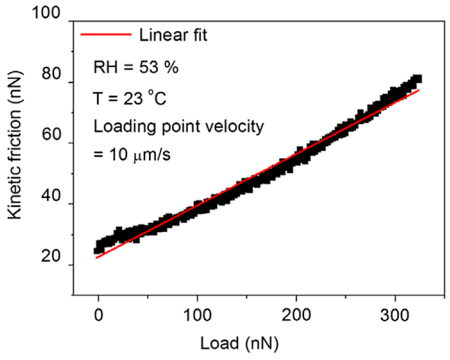

FIG. 3. Kinetic friction vs normal load. The silica substrate was cleaned with a piranha solution before the experiment. The load is systematically varied from 0 to 325 nN.

The physical picture represented by linearized Eq. (5) (the load and time dependence of aging) can be understood as follows: the load dependence $(\frac{2}{3}L + L_0)$ approximately determines the number of initial available reaction sites (proportional to the contact area), setting the stage for the ensuing aging process; the time dependence $[2.3\log(t) - 2.3\log(\tau_0) + 0.58]$ describes how the interfacial chemical bonds per unit contact area form with time. A larger load creates a larger number of sites for aging to occur (i.e., where siloxane bonds can form), while, on average, it does not affect the formation kinetics of individual chemical bonds.

Although the area-load dependence is explicitly nonlinear in the DMT model and this is also likely the case in our actual experiment, the nonlinearity resulting from Eq. (3) is rather small over the constrained load regime we can access (Fig. 2 and Fig. S5), indicating that the potentially complex effects of the load on both the contact area and the energy barrier [i.e., the term N/G in Eq. (2)] end up varying nearly linearly with the load. In other words, while the number of available reaction sites and the energy barrier distribution all have different load dependences (and the energy barrier distribution varies with the hold time), they combine in a way that leads to an approximately linear variation with the load, independent of the hold time. While simple, our approaches [Eqs. (4) and (5) for the linear approximation and Eq. (3) for the more accurate nonlinear version] provide a first approximate method to analyze the load dependence of friction for an aging contact. From the analysis, we extract the energy barrier and the activation volume (i.e., the stress sensitivity of the energy barrier) for the nanoscale silica-silica aging process.

Now we discuss the possible relationship between nanoscale ICBI friction, macroscale friction, and the macroscopic RSF laws. For materials like polymer glasses, it has been shown experimentally that the real contact area (as measured optically with a resolution of micrometers) increases logarithmically with time [48]. In this case, chemical bonds may not play an important role at the macroscale. This can be explained as follows. For a logarithmic increase of the number of chemical bonds with time for a given real contact area, the *rate* of bond formation *decreases* with time. Therefore, within any time interval, the bonds in the newly formed contact area (i.e., those formed in that time interval) have a higher growth rate than the bonds in the previously formed area (i.e., that formed before this time interval). Thus, the total number of chemical bonds formed should increase in a way that is faster than the logarithmic increase with time. So, as long as the increase of the real contact area is comparable to or greater than the rate of chemical bond formation, chemical bonding cannot be the main reason for macroscale aging.

On the other hand, for materials like rocks, an increase in the real area of contact during hold experiments has not been demonstrated, due to the high yield strength of silicate minerals and the resulting microscopic to submicroscopic asperity sizes, which cannot be measured precisely using, for example, optical techniques [49]. Indirect methods,

using measurements of acoustic impedance normal to the frictional interface during hold experiments, indicate an increase in the real contact area with the hold time [50]. The difficulty of determining the increase in the contact area during aging for rocks is compounded by the usual presence of wear debris, or "gouge," on the frictional interface, which contains myriad microscopic to submicroscopic frictional contacts. For these reasons, the relative contributions of asperity creep and chemical bond formation on macroscopic rock friction remain unknown.

It is important to discuss the feasibility that interfacial chemical bonds could form on a macroscale contact based on our results. In our nanoscale experiments, the aging phenomenon is sensitive to surface cleanliness. As shown in Ref. [18], if the tip is taken out of contact from the surface for some time, aging is suppressed due to contamination. However, if the tip is scanned first, the contact is refreshed and shows aging. This effect may be due to the removal of hydrocarbon groups or other contaminants from the interface that came from the atmosphere and/or from freshly exposing bonds on the tip due to bond breaking induced by scanning. We propose such a refreshment could happen for macroscale contacts, since a macroscale sliding interface is refreshing its asperity population all the time [5].

In conclusion, we show that the friction drop for aged silica-silica contacts is approximately proportional to the product of the normal load and the log of the hold time above ~0.1 s contact time, in the positive load regime. With respect to the load and time dependence of aging in macroscale contacts, we propose that, for those contact regions where the deformation is elastic [51], our model of the nanoscale aging might be applied as a potential mechanism. More generally, our work connects the chemical kinetics and contact mechanics, provides further evidence that nanoscale RSF behavior originates from interfacial chemical bond formation, and establishes the applicability of RSF laws for nanoscale single-asperity contacts.

We thank A. Li, M. O. Robbins, and X. Liu for useful discussions. We acknowledge funding from the National Science Foundation under Grants No. EAR-1141142, No. EAR-1141882, No. EAR-1549153, and No. EAR-1550112. K. T. and N. N. G. prepared the tips and substrates, performed experiments, and obtained and analyzed the data with input from all other authors. All six authors wrote this manuscript together.

*Corresponding author.
carpick@seas.upenn.edu
†Present address: Department of Applied Mechanics, IIT Delhi, Hauz Khas, New Delhi 110016, India.

[1] A. D. Corwin and M. P. de Boer, Frictional aging and sliding bifurcation in monolayer-coated micromachines, J. Microelectromech. Syst. **18**, 250 (2009).
[2] A. D. Corwin and M. P. de Boer, Frictional aging, de-aging, and re-aging in a monolayer-coated micromachined interface, Phys. Rev. B **81**, 174109 (2010).
[3] S. S. Shroff, N. Ansari, W. R. Ashurst, and M. P. de Boer, Rate-state friction in microelectromechanical systems interfaces: Experiment and theory, J. Appl. Phys. **116**, 244902 (2014).
[4] J. H. Dieterich, Time-dependent friction in rocks, J. Geophys. Res. **77**, 3690 (1972).
[5] J. H. Dieterich, Modeling of rock friction: 1. Experimental results and constitutive equations, J. Geophys. Res. **84**, 2161 (1979).
[6] J. R. Rice and A. L. Ruina, Stability of steady frictional slipping, J. Appl. Mech. **50**, 343 (1983).
[7] N. M. Beeler, T. E. Tullis, and J. D. Weeks, The roles of time and displacement in the evolution effect in rock friction, Geophys. Res. Lett. **21**, 1987 (1994).
[8] C. Marone, Laboratory-derived friction laws and their application to seismic faulting, Annu. Rev. Earth Planet Sci. **26**, 643 (1998).
[9] P. Berthoud, T. Baumberger, C. G'Sell, and J.-M. Hiver, Physical analysis of the state-and rate-dependent friction law: Static friction, Phys. Rev. B **59**, 14313 (1999).
[10] T. Baumberger, P. Berthoud, and C. Caroli, Physical analysis of the state-and rate-dependent friction law. II. Dynamic friction, Phys. Rev. B **60**, 3928 (1999).
[11] F. Heslot, T. Baumberger, B. Perrin, B. Caroli, and C. Caroli, Creep, stick-slip, and dry-friction dynamics: Experiments and a heuristic model, Phys. Rev. E **49**, 4973 (1994).
[12] J. H. Dieterich, Constitutive properties of faults with simulated gouge, in Mechanical Behavior of Crustal Rocks: The Handin Volume (American Geophysical Union, Washington, DC, 1981).
[13] J. R. Rice, Constitutive relations for fault slip and earthquake instabilities, Pure Appl. Geophys. **121**, 443 (1983).
[14] T. E. Tullis and J. D. Weeks, *Constitutive Behavior and Stability of Frictional Sliding of Granite, in Friction and Faulting* (Springer, New York, 1987), p. 383.
[15] F. Bowden and D. Tabor, The area of contact between stationary and between moving surfaces, Proc. R. Soc. A **169**, 391 (1939).
[16] I. Szlufarska, M. Chandross, and R. W. Carpick, Recent advances in single-asperity nanotribology, J. Phys. D **41**, 123001 (2008).
[17] J. Weeks, N. Beeler, and T. Tullis, Glass is like a rock, Eos Trans. AGU **72**, 457 (1991).
[18] Q. Li, T. E. Tullis, D. Goldsby, and R. W. Carpick, Frictional ageing from interfacial bonding and the origins of rate and state friction, Nature (London) **480**, 233 (2011).
[19] Y. Liu and I. Szlufarska, Chemical Origins of Frictional Aging, Phys. Rev. Lett. **109**, 186102 (2012).
[20] G. Vigil, Z. Xu, S. Steinberg, and J. Israelachvili, Interactions of silica surfaces, J. Colloid Interface Sci. **165**, 367 (1994).
[21] A. Li, Y. Liu, and I. Szlufarska, Effects of interfacial bonding on friction and wear at silica/silica interfaces, Tribol. Lett. **56**, 481 (2014).
[22] See Supplemental Material at http://link.aps.org/supplemental/10.1103/PhysRevLett.118.076103 for details

of sample preparation, derivations of equations, simulation results and other discussions, which includes Refs. [23–36].

[23] S. Rhee, Surface energies of silicate glasses calculated from their wettability data, J. Mater. Sci. **12**, 823 (1977).

[24] B. V. Derjaguin, V. M. Muller, and Y. P. Toporov, Effect of contact deformations on the adhesion of particles, J. Colloid Interface Sci. **53**, 314 (1975).

[25] T. H. Elmer, *Porous and Reconstructed Glasses*, Engineered Materials Handbook Vol. 4 (ASM International, Metals Park, OH, 1991), p. 427.

[26] L. Dongmo, J. S. Villarrubia, S. N. Jones, T. B. Renegar, M. T. Postek, and J. F. Song, Experimental test of blind tip reconstruction for scanning probe microscopy, Ultramicroscopy **85**, 141 (2000).

[27] K. Johnson, Non-Hertzian contact of elastic spheres, in *The Mechanics of Contact Between Deformable Solids*, edited by A. D. de Pater and J. J. Kalker (Delft University Press, Delft, 1975), pp. 26–40.

[28] R. W. Carpick, D. F. Ogletree, and M. Salmeron, A general equation for fitting contact area and friction vs load measurements, J. Colloid Interface Sci. **211**, 395 (1999).

[29] C. M. Mate, *Tribology on the Small Scale* (Oxford University, New York, 2008).

[30] D. S. Grierson, E. E. Flater, and R. W. Carpick, Accounting for the JKR–DMT transition in adhesion and friction measurements with atomic force microscopy, J. Adhes. Sci. Technol. **19**, 291 (2005).

[31] J. Greenwood, Adhesion of elastic spheres, Proc. R. Soc. A **453**, 1277 (1997).

[32] J. E. Sader, J. W. M. Chon, and P. Mulvaney, Calibration of rectangular atomic force microscope cantilevers, Rev. Sci. Instrum. **70**, 3967 (1999).

[33] C. P. Green, H. Lioe, J. P. Cleveland, R. Proksch, P. Mulvaney, and J. E. Sader, Normal and torsional spring constants of atomic force microscope cantilevers, Rev. Sci. Instrum. **75**, 1988 (2004).

[34] E. Meyer, H. J. Hug, and R. Bennewitz, *Scanning Probe Microscopy: The Lab on a Tip* (Springer, New York, 2004).

[35] Q. Li, K.-S. Kim, and A. Rydberg, Lateral force calibration of an atomic force microscope with a diamagnetic levitation spring system, Rev. Sci. Instrum. **77**, 065105 (2006).

[36] J. Procelewska, A. Zahl, R. van Eldik, H. A. Zhong, J. A. Labinger, and J. E. Bercaw, Activation volume measurement for CH activation. Evidence for associative benzene substitution at a platinum (II) center, Inorg. Chem. **41**, 2808 (2002).

[37] Y. Mo, K. T. Turner, and I. Szlufarska, Friction laws at the nanoscale, Nature (London) **457**, 1116 (2009).

[38] Y. Mo and I. Szlufarska, Roughness picture of friction in dry nanoscale contacts, Phys. Rev. B **81**, 035405 (2010).

[39] P. Schwaderer, E. Funk, F. Achenbach, J. Weis, C. Bräuchle, and J. Michaelis, Single-molecule measurement of the strength of a siloxane bond, Langmuir **24**, 1343 (2008).

[40] T. D. Jacobs and R. W. Carpick, Nanoscale wear as a stress-assisted chemical reaction, Nat. Nanotechnol. **8**, 108 (2013).

[41] G. Gibbs, The thermodynamics of thermally-activated dislocation glide, Phys. Status Solidi (b) **10**, 507 (1965).

[42] G. Taylor, Thermally-activated deformation of BCC metals and alloys, Prog. Mater. Sci. **36**, 29 (1992).

[43] D. Ogletree, R. W. Carpick, and M. Salmeron, Calibration of frictional forces in atomic force microscopy, Rev. Sci. Instrum. **67**, 3298 (1996).

[44] M. Varenberg, I. Etsion, and G. Halperin, An improved wedge calibration method for lateral force in atomic force microscopy, Rev. Sci. Instrum. **74**, 3362 (2003).

[45] J. Gao, W. D. Luedtke, D. Gourdon, M. Ruths, J. N. Israelachvili, and U. Landman, Frictional forces and Amontons' law: From the molecular to the macroscopic scale, J. Phys. Chem. B **108**, 3410 (2004).

[46] M. Lessel, P. Loskill, F. Hausen, N. N. Gosvami, R. Bennewitz, and K. Jacobs, Impact of van der Waals Interactions on Single Asperity Friction, Phys. Rev. Lett. **111**, 035502 (2013).

[47] E. E. Flater, W. R. Ashurst, and R. W. Carpick, Nanotribology of octadecyltrichlorosilane monolayers and silicon: Self-mated versus unmated interfaces and local packing density effects, Langmuir **23**, 9242 (2007).

[48] J. H. Dieterich and B. D. Kilgore, Direct observation of frictional contacts: New insights for state-dependent properties, Pure Appl. Geophys. **143**, 283 (1994).

[49] J. H. Dieterich and B. D. Kilgore, Imaging surface contacts: Power law contact distributions and contact stresses in quartz, calcite, glass and acrylic plastic, Tectonophysics **256**, 219 (1996).

[50] K. Nagata, M. Nakatani, and S. Yoshida, Monitoring frictional strength with acoustic wave transmission, Geophys. Res. Lett. **35**, L06310 (2008).

[51] K. M. Frye, Effect of humidity on granular friction at room temperature, J. Geophys. Res. **107**, ETG 11-1 (2002).